PERGAMON

Computers and Structures 80 (2002) 1667–1687

Computers & Structures

www.elsevier.com/locate/compstruc

A finite element methodology for local/global damage evaluation in civil engineering structures

Alex D. Hanganu [a], Eugenio Oñate [a,b,*], Alex H. Barbat [b]

[a] *International Centre for Numerical Methods in Engineering, Universidad Politecnica de Cataluna, Gran Capitán s/n, 08034 Barcelona, Spain*

[b] *ETS Ingenieros de Caminos, Canales y Puertos Universidad Politécnica de Cataluña, 08034 Barcelona, Spain*

Received 19 June 2001; accepted 20 January 2002

Abstract

The paper introduces a new global damage evaluation method which leads to a meaningful global damage index. A numerical procedure for the prediction of local and global damage in civil engineering structures using the finite element method and a continuum damage model, is presented. The method is adequate for the computation of the limit load in reinforced concrete (RC) structures and for the prediction of the failure mechanisms. Details of the applied damage model are given together with a description of the finite element implementation and the procedure for computing the global damage parameters. Examples of applications of the methodology to the nonlinear analysis of a range of RC structures, are presented.

Keywords: Structural global damage; Damage models; Reinforced concrete structures; Failure load; Failure mechanisms; Nonlinear analysis; Finite element method

1. Introduction

Since in the 1980s structural analysis was performed including material nonlinearity in the study and design of civil engineering structures, engineers gained access to detailed information regarding phenomena occurring beyond material elastic limit. This information typically describes the state of the material on a point by point basis, but is not easy to extrapolate to the entire structure nor offers sufficient indications about its general state. Furthermore, the relevance to overall structural stability and serviceability of the fact that a certain part of a structure is more or less damaged, is difficult to infer from the local information provided by classical nonlinear constitutive models.

The study at macroscopic scale of concrete behaviour was traditionally founded on crack models for tension and crush models for compression [19]. A latter-day popular viable alternative are the damage models that bring about a unified treatment of concrete behaviour under both tension and compression.

Damage models may be classified mainly into two families: those employed mostly in seismic engineering for beam structures, evaluating damage indices from parameters like sectional forces, ductility or deformational energy of structural members [4,25,35]; the second family is made up by the continuum mechanics damage models that describe the material state of a point of the structure and are based on the principles of thermodynamics [20,21,23,24,26,27].

The structural damage is defined as the degree of degradation that allows conclusions about the capacity of a structure to withstand further loadings. It is usually quantified through damage indices that represent actual

* Corresponding author. Address: International Centre for Numerical Methods in Engineering, Universidad Politecnica de Cataluna, Gran Capitán s/n, 08034 Barcelona, Spain. Tel.: +34-93-205-7016; fax: +34-93-401-6517.

E-mail address: onate@cimne.upc.es (E. Oñate).

0045-7949/02/$ - see front matter
PII: S0045-7949(02)00012-3

damage normalised to the failure level of the structure. A value of the damage index equal to 1 reflects complete loss of strength while a value of 0 means no damage.

The attributes "local" and "global" are often associated with damage indices in current terminology. In general acceptance, a damage index is local when it refers to a single point, sections, members or structural parts, while it is considered global when it describes the state of an entire structure.

The need for damage indices as an evaluation tool was acknowledged since the 1970s mainly in seismic engineering in whose realm many formulae for beam structures were developed [4,25,35]. These formulae for "local" damage indices are based on concepts like cumulative plastic deformations under cyclic loading [4], ratios between absolute maximum bending moments and maximum bending moments reached during the earthquake [25] or the currently extensively employed function of Park and Ang [36], linking linearly structural member ductility with dissipated energy under cyclic loading. All these indices are adequate for seismic analyses but are not applicable directly to other types of studies.

The definitions of global damage indices generally rely on weighted averages of "local" (partial) indices. The proposed weighting factors vary widely from member volume or quota of potential energy absorbed by the member, to esoteric criteria like the assignment by experts of relative importance factors to the various structural subparts.

DiPasquale and Çakmak [13–15] proposed the first objective global damage index definition based on less empirical concepts, as a function of the variation of the fundamental frequency of the structure. This sound basis provides an accurate description of the state of an entire structure but it presents two major drawbacks. First, it cannot be applied to determine the damage of a substructure (ex. a storey of a building) and its impact on the overall behaviour. Secondly, it requires the evaluation of the fundamental frequency for each load increment. This involves costly calculations of tangent stiffness matrices that, on the other hand, are not always known and sometimes do not even exist.

The damage evaluation methodology presented in this paper addresses the following problems considered of high interest for structural engineering:

1. Synthetic evaluation of the damage state of an entire structure and of any of its parts, during and after static or dynamic actions which drive the constitutive materials beyond the elastic threshold.
2. Failure load evaluation for complex structures.
3. Reliability, safety and structural health assessment.

The proposed global damage evaluation method is based on continuum mechanics principles, henceforth the label "local" will be applied only to damage indices describing the state of the material at particular points of the structure while the "global" damage indices will refer to the state of any finite volume of material. Thus, global damage indices for individual finite elements, substructures or the whole structure will be discussed. This new classification is justified by the fact that in continuum mechanics the constitutive models are applied at point level and all other magnitudes are obtained integrating pointwise data.

The global damage evaluation theory presented herein may operate independently from the chosen constitutive models for the structural materials. Hence it is always possible to obtain global damage indices whatever the local constitutive model may be. This feature converts the proposed global damage index (GDI) into a powerful general tool for structural assessment. Moreover, it is applicable directly to both static and dynamic analyses.

The paper is organised as follows: In the next sections the theoretical bases of the damage model are introduced to act as supporting theory for the global damage methodology. The finite element implementation is briefly outlined. Examples of application of the methodology to nonlinear analysis of a range of RC structures, such as a simple RC frame, a complete storey of a housing building and a nuclear containment shell, are finally presented.

2. The concept of damage

Extensive experimental studies have been undertaken to characterise the response and the ultimate strength of plain concrete under multi-axial stress states [2,3,22,40]. Considerable scatter of results has been observed and collaborative studies have been undertaken to identify the principal factors influencing this variation [2,29]. Several approaches, based on experimental data, have been used to represent the constitutive relationship under multi-axial stresses and these can be categorised into the five following groups: (a) linear and nonlinear elasticity theories, (b) perfect and work-hardening and softening plasticity theories, (c) endochronic theory of plasticity, (d) plastic fracturing theory and damage theory and, (e) damage theory.

A simple and popular model for nonlinear finite element analysis of concrete structures assumes elasto-plastic (or viscoplastic) constitutive equations for compression behaviour, whereas a conceptually more simple smeared elasto-brittle model is used for defining onset and progression of cracks at points in tension. Different versions of this model have been successfully used for nonlinear analysis of plain and reinforced concrete (RC) structures. A summary of some of the more recent contributions in each of those theories can be found in [29,31,32,38].

The elasto-plastic-brittle smeared model, in spite of its popularity, presents various controversial features such as the need for defining uncoupled behaviour along each principal stress (or strain) directions: the use of a shear retention factor to ensure some shear resistance along the crack; the lack of equilibrium at the cracking point when more than one crack is formed; the difficulties in defining stress paths following the opening and closing of cracks under cycling loading conditions and the difficulty for dealing with the combined effect of cracking and plasticity at the damaged points. It should be noted that the description of compressive and tensile behaviours on the basis of plasticity theory circumvents the described disadvantages [41].

It is well known that micro-cracking in concrete and masonry takes place at low load levels due to physical de-bonding between aggregate and mortar particles, or to simple micro-cracking in the mortar area. Cracking progresses following a nonhomogeneous path which combines the two mentioned mechanisms, with growth and linking between micro-cracks along different directions. Experiments carried out on mortar specimens show that the distribution of micro-cracking is fairly discontinuous with arbitrary orientations [1,3]. This fact is supported by many experiments which show that cracking can be considered at microscopic level as a nondirectional phenomenon and that the propagation of micro-cracks follows an erratic path which depends on the size of the aggregate particles. Thus, the dominant cracking directions can be interpreted at macroscopic level as the locus of trajectories of the damage points (Fig. 1).

The above concepts support the idea that *the nonlinear behaviour of concrete can be modelled using concepts of damage theory only* [21,23,26,31,33,37], provided an adequate damage function is defined for taking into account the different response of concrete under tension and compression states. Cracking can, therefore, be interpreted as a *local damage effect*, defined by the evolution of known material parameters and by one or several functions which control the onset and evolution of damage.

One of the advantages of such a model is the independence of the analysis with respect to cracking directions which can be simply identified *a posteriori* once the nonlinear solution is obtained. This allows to overcome the problems associated with most elastic-plastic-brittle smeared cracking models. In this paper a model developed in recent years by the authors group in [5,10–12,16–18,27,30–33] for nonlinear analysis of concrete based on the concept of *damage* mentioned above, is presented. The model takes into account all the important aspects which should be considered in the nonlinear analysis of concrete and masonry structures such as the different response under tension and compression, the effect of stiffness degradation due to mechanical effects

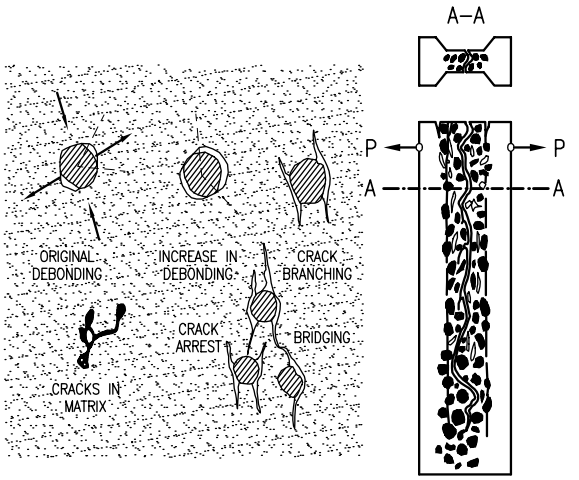

Fig. 1. Mechanics of damage and propagation of a macroscopic crack in plain concrete.

and the problem of objectivity of the results with respect to the finite element mesh.

In order to clarify the concept of damage, let us consider a surface element in a damaged material volume. This surface has an area large enough to contain a representative number of defects, but still enabling to be referred as pertaining to a particular material point. Thus, if S_n denotes the overall section and $\overline{S}_n$ the effective resisting area ($S_n - \overline{S}_n$ is the area occupied by the voids), the *damage variable* d_n associated with this surface is

$$d_n = \frac{S_n - \overline{S}_n}{S_n} = 1 - \frac{\overline{S}_n}{S_n} \tag{2.1}$$

Clearly, d_n represents the surface density of material defects and it will have a zero value when the material is in the undamaged virgin state. Conversely, the reduction of the effective resisting area will lead to an increase of damage until rupture defined by some critical value of d_n (bounded by the unreachable value of $d_n = 1$). Note that this is a directional definition of damage. In many cases a single scalar representation of damage is adopted (i.e. $d_n = d$) which suffices to ensure realistic material modelling. It is worth noting, that in this case cracks at a microscopic point need have no particular direction and a macroscopic crack is then defined as the locus of damage points.

A useful concept for understanding the effect of damage is that of *effective stress*. The equilibrium relationship between the standard Cauchy stress σ and the "effective" stress, $\bar{\sigma}$, in the damaged bar specimen of Fig. 2 is

$$\sigma S = \bar{\sigma}\overline{S} \tag{2.2}$$

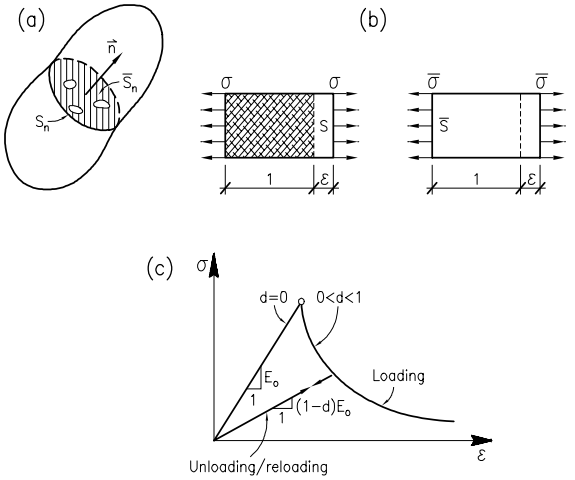

Fig. 2. (a) Damaged surface, (b) Cauchy σ and effective $\bar{\sigma}$ stresses and (c) uniaxial stress–strain curve.

and from (2.1) and (2.2)

$$\sigma = (1-d)\bar{\sigma} = (1-d)E\varepsilon \tag{2.3}$$

When a damaging process is occurring, the external loading is resisted by the effective stress area and, therefore, $\bar{\sigma}$ is a more physically representative parameter than σ. Note that the Cauchy stress vanishes when the damage parameter approaches unity. Eq. (2.3) also allows to identify an equivalent Young Modulus $\overline{E} = (1-d)E$ which also tends to zero as $d \to 1$ (Fig. 2).

3. Damage constitutive model

3.1. General concepts

The first formulations started from representing the behaviour of materials in an approximate form based mainly on experimental studies. Today, it is required that these formulations be thermodynamically consistent. Among those meeting this requirement, the so-called continuous damage theory is generally accepted as an alternative in the most complex constitutive formulations [14,30]. The damage models have a rigorous but relatively simple formulation strictly based on thermodynamics [39]. They deal with the nonlinear behaviour by means of one or more internal variables called damage variables, which indicate the loss of secant stiffness of the material and are normalised to a unit value which corresponds to maximum damage. Fig. 3 shows a simplified unidimensional representation of the behaviour of a point within a damaged material [30].

The model presented herein is a 3D damage constitutive model based on solid mechanics and it has a single

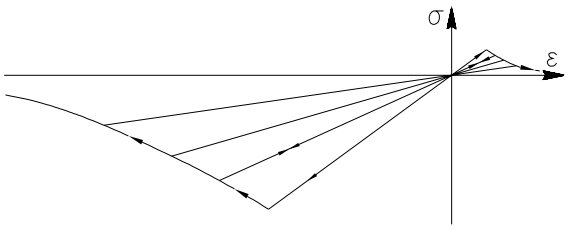

Fig. 3. Local damage behaviour.

internal variable [30]. Therefore, this is a local isotropic damage model and it is based on Kachanov's theory [20], appropriate for simulating the behaviour of concrete under monotonically increasing loads. Many ideas inherent to the model have been taken from the works of Simó and Ju [39], Lubliner et al. [27] and Oliver et al. [30]. This formulation has been chosen because it is a compromise between the complexity of the models describing the behaviour of the concrete and the versatility needed when dealing with dynamic problems. This insures accurate results and low cost solutions for the nonlinear problems which are the object of this paper.

The numerical treatment of viscoelastic phenomena in materials can be followed in detail in Lubliner [28] and Simó and Hughes [39]. The damping effect of the structure is simulated in this work by using a model consisting of a damper placed in parallel with the structure [6].

3.2. Characteristics of the damage model

3.2.1. Free energy and constitutive law

The model is formulated in the material configuration, for thermodynamically stable problems with no temperature time variation. For this specific case the following mathematical form for the free energy is assumed, where the nondamaged elastic part is expressed as a scalar quadratic function of tensorial arguments [30,37]

$$\begin{aligned}\Psi(\varepsilon;d) &= (1-d)\Psi_0(\varepsilon) = (1-d)\left(\frac{1}{2\rho_0}\varepsilon^{\mathrm{T}}\boldsymbol{\sigma}^0\right)\\ &= (1-d)\left(\frac{1}{2\rho_0}\varepsilon^{\mathrm{T}}\boldsymbol{C}^0\varepsilon\right)\end{aligned} \tag{3.1}$$

In Eq. (3.1) the strain tensor ε is the free variable of the problem, $d\,(0 \leqslant d \leqslant 1)$ is the internal damage variable, ρ_0 is the density in the material configuration and $\boldsymbol{C}^0$ is the stiffness tensor of the material in the initial undamaged state.

For stable thermal state problems the Clasius Planck dissipation inequality is valid, whose local Lagrangian form is [28]

$$\dot{\Xi}_m = \frac{1}{\rho_0}\sigma^{\mathrm{T}}\dot{\varepsilon} - \dot{\Psi} \geqslant 0 \tag{3.2}$$

$$\dot{\Xi}_m = \left(\frac{1}{\rho_0}\boldsymbol{\sigma}^{\mathrm{T}} - \frac{\partial \Psi}{\partial \varepsilon}\right)\dot{\varepsilon} - \frac{\partial \Psi}{\partial d}\dot{d} \geqslant 0 \tag{3.3}$$

This expression for the dissipation rate $\dot{\Xi}_m$ allows the following two considerations:

(a) In order to guarantee the unconditional fulfilment of the Clasius Planck inequality [28], the multiplier of $\dot{\varepsilon}$ which represents an arbitrary temporal variation of the free variable, must be null. This condition provides the constitutive law of the damage model:

$$\frac{1}{\rho_0}\boldsymbol{\sigma}^{\mathrm{T}} - \frac{\partial \Psi}{\partial \varepsilon} = 0 \Rightarrow \boldsymbol{\sigma} = \rho_0\left\{\frac{\partial \Psi}{\partial \varepsilon}\right\}^{\mathrm{T}} = (1-d)\boldsymbol{C}^0\varepsilon = \boldsymbol{C}^S\varepsilon \tag{3.4}$$

$$\boldsymbol{C}^S = (1-d)\boldsymbol{C}^0$$

where $\boldsymbol{C}^S$ is the secant stiffness tensor.

(b) Inserting the last equation into (3.3), the dissipation rate is now given by

$$\dot{\Xi}_m = -\frac{\partial \Psi}{\partial d}\dot{d} = \Psi_0\dot{d} \geqslant 0 \tag{3.5}$$

As Ψ_0 is always positive, Eq. (3.5) states that the damage rate $\dot{d}$ cannot be negative, i.e. the damage level can only stay constant or increase and never decrease.

3.2.2. Damage criterion

The damage criterion is defined as a function of the free energy of the undamaged material, expressed in terms of the undamaged principal stresses $\sigma_i^{\mathrm{p},0}$, as

$$F = K(\boldsymbol{\sigma}^{\mathrm{p},0})\sqrt{2\rho_0\Psi_0} - 1 = \frac{K(\boldsymbol{\sigma}^{\mathrm{p},0})}{\sqrt{E^0}}\sqrt{\sum_{i=1}^{3}(\sigma_i^{\mathrm{p},0})^2} - 1 \leqslant 0 \tag{3.6}$$

where the terms of the above equation have the following meaning:

$$K(\boldsymbol{\sigma}^{\mathrm{p},0}) = \frac{r}{\sqrt{2\rho_0(\Psi_{\mathrm{t}}^0)_L}} + \frac{1-r}{\sqrt{2\rho_0(\Psi_{\mathrm{c}}^0)_L}}; \quad r = \frac{\sum_{i=1}^{3}\langle\sigma_i^{\mathrm{p},0}\rangle}{\sum_{i=1}^{3}|\sigma_i^{\mathrm{p},0}|}$$

$$2\rho_0(\Psi_{\mathrm{t,c}}^0)_L = \sum_{i=1}^{3}\langle\pm\sigma_i^{\mathrm{p},0}\rangle\varepsilon_i; \quad (\Psi_0)_L = (\Psi_{\mathrm{t}}^0)_L + (\Psi_{\mathrm{c}}^0)_L$$

In these equations $(\Psi_{\mathrm{t,c}}^0)_L$ represent the part of the free energy developed when the tension/compression limit is reached and $\langle\pm x\rangle = \frac{1}{2}(|x| \pm x)$ is the McAuley's function. Taking into account that the tension and compression strengths are $f_{\mathrm{t}} = (2\rho_0\Psi_{\mathrm{t}}^0E^0)_L^{1/2}$ and $f_{\mathrm{c}} = (2\rho_0\Psi_{\mathrm{c}}^0E^0)_L^{1/2}$ respectively, and substituting the last definition in the Eq. (3.6), the damage function can be written, according to Fig. 4, as

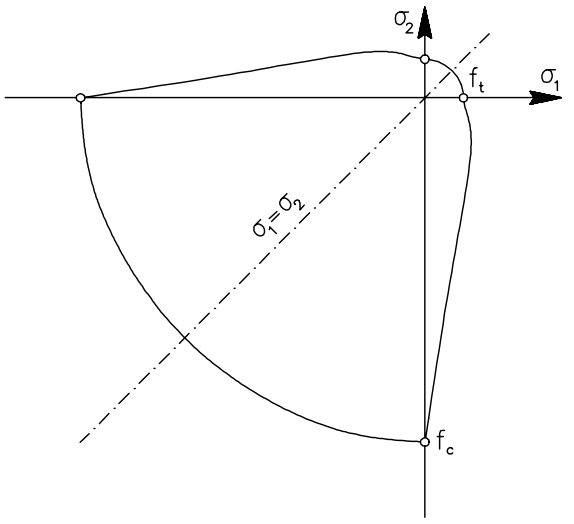

Fig. 4. Damage yield function in the principal stress plane $\sigma_1 - \sigma_2$.

$$F = \bar{\sigma} - f_{\mathrm{c}} \leqslant 0 \tag{3.7}$$

where

$$\bar{\sigma} = [1 + r(n-1)]\sqrt{\sum_{i=1}^{3}(\sigma_i^{\mathrm{p},0})^2} \tag{3.8}$$

with $n = f_{\mathrm{c}}/f_{\mathrm{t}}$. This damage function, expressed in the nondamaged principal stresses space, allows a great number of choices. The advantage of the yield criterion written in Eq. (3.8) is that any yield function F can be used always as long as it is homogeneous and of first order in stresses (i.e. Mohr–Coulomb, Drucker–Prager, Lubliner et al. [27], etc.), in substitution of the equivalent stress $\bar{\sigma}$.

This opens the possibility of applying more accurate and powerful theories within the theoretical framework given by Eq. (3.7). Nevertheless, the simple form provided by Eq. (3.8) fulfils the above requirements; besides, it is simple and yields satisfactory results within the range of assumptions made for this model and therefore will be used henceforward as the scalar expression defining $\bar{\sigma}$ [30]. Simó and Ju [37] proposed a very convenient expression entirely equivalent to (3.7)

$$\overline{F} = G(\bar{\sigma}) - G(f_{\mathrm{c}}) \leqslant 0 \tag{3.9}$$

where $G(\chi)$ is a scalar monotonic function to be determined. Its shape is to be chosen suitably to the subsequent development of the damage model.

3.2.3. Evolution of the damage variable

The following evolution law is used for the damage internal variable:

$$\dot{d} = \dot{\mu}\frac{\partial \overline{F}}{\partial \bar{\sigma}} = \dot{\mu}\frac{\mathrm{d}G(\bar{\sigma})}{\mathrm{d}\bar{\sigma}} \tag{3.10}$$

where $\dot{\mu}$ is a nonnegative damage consistency parameter, analogous to the plastic consistency parameter $\dot{\lambda}$ in standard plasticity theory.

Similarly to plasticity, a yielding criterion $\overline{F} = 0$ and a consistency condition $\dot{\overline{F}} = 0$ for a point subjected to a damaging process are defined. The yielding rule and the properties of $G(\chi)$ allow to write $G(\bar{\sigma}) - G(f_c) = 0$, what implies $\bar{\sigma} = f_c$ and consequently

$$\frac{\mathrm{d}G(\bar{\sigma})}{\mathrm{d}\bar{\sigma}} = \frac{\mathrm{d}G(f_c)}{\mathrm{d}f_c} \tag{3.11}$$

From the condition of consistency—that means persistency on the damage surface—and from the properties of function $G(\chi)$, the following equation is deduced:

$$\frac{\partial \overline{F}}{\partial \bar{\sigma}}\dot{\bar{\sigma}} + \frac{\partial \overline{F}}{\partial f_c}\dot{f}_c = \frac{\mathrm{d}G(\bar{\sigma})}{\mathrm{d}\bar{\sigma}}\dot{\bar{\sigma}} - \frac{\mathrm{d}G(f_c)}{\mathrm{d}f_c}\dot{f}_c = 0 \tag{3.12}$$

and the use of (3.11) allows to write $\dot{\bar{\sigma}} = \dot{f}_c$. Eq. (3.12) can be now rewritten and leads to

$$\begin{aligned}\frac{\mathrm{d}G(\bar{\sigma})}{\mathrm{d}\bar{\sigma}}\dot{\bar{\sigma}} &= \frac{\mathrm{d}G(f_c)}{\mathrm{d}f_c}\dot{f}_c = \frac{\mathrm{d}G(f_c)}{\mathrm{d}f_c}\frac{\mathrm{d}f_c}{\mathrm{d}(d)}\dot{d} \\ &= \frac{\mathrm{d}G(f_c)}{\mathrm{d}(d)}\dot{\mu}\frac{\mathrm{d}\overline{G}(\bar{\sigma})}{\mathrm{d}\bar{\sigma}}\end{aligned} \tag{3.13}$$

$$\dot{\bar{\sigma}} = \frac{\mathrm{d}G(f_c)}{\mathrm{d}(d)}\dot{\mu} \tag{3.14}$$

Conveniently choosing $G(f_c)$ as the function which describes the evolution of the damage $[d = G(f_c)]$, the damage consistency parameter $\dot{\mu}$ can be expressed as

$$\dot{\mu} = \dot{\bar{\sigma}} = \dot{f}_c = \frac{\partial \bar{\sigma}}{\partial \boldsymbol{\sigma}^0}\dot{\boldsymbol{\sigma}}^0 = \frac{\partial \bar{\sigma}}{\partial \boldsymbol{\sigma}^0}\boldsymbol{C}^0\dot{\boldsymbol{\varepsilon}} \tag{3.15}$$

Substituting this equation into (3.10) and (3.5), the following expressions which govern the temporal evolution of the damage and dissipation variables are obtained:

$$\dot{d} = \frac{\mathrm{d}G(\bar{\sigma})}{\mathrm{d}\bar{\sigma}}\dot{\bar{\sigma}} \tag{3.16}$$

$$\begin{aligned}\dot{\Xi}_m &= \Psi_0\dot{G}(\bar{\sigma}) = \Psi_0\frac{\mathrm{d}G(\bar{\sigma})}{\mathrm{d}\bar{\sigma}}\dot{\bar{\sigma}} \\ &= \Psi_0\frac{\mathrm{d}G(\bar{\sigma})}{\mathrm{d}\bar{\sigma}}\frac{\partial \bar{\sigma}}{\partial \boldsymbol{\sigma}^0}\boldsymbol{C}^0\dot{\boldsymbol{\varepsilon}}\end{aligned} \tag{3.17}$$

The loading/unloading condition is derived from the relations of Kuhn–Tucker formulated for problems with unilateral restrictions: (a) $\dot{\mu} \geqslant 0$; (b) $\overline{F} \leqslant 0$ and (c) $\dot{\mu}\overline{F} = 0$. From these, if $\overline{F} < 0$, then the third condition imposes $\dot{\mu} = 0$ and, if $\dot{\mu} > 0$, then the same condition requires that $\overline{F} = 0$.

3.2.4. Definition of function G

From the different alternatives for defining function $G(\chi)$ [37], the following equation was chosen here

$$G(\chi) = 1 - \frac{\overline{G}(\chi)}{\chi} \tag{3.18}$$

where $\overline{G}(\chi)$ describes a function so that it gives for $\chi = \chi^*$ the initial yield stress $\overline{G}^*$ and for $\chi \to \infty$ the final strength $\overline{G} \to 0$. Thus, by running all the deformation path, the point will have dissipated an energy equivalent to the specific fracture energy. In our work, the exponential function proposed by Oliver et al. [30], which is shown in Fig. 5, was used

$$\overline{G}(\chi) = \chi^* \mathrm{e}^{A\left(1-\frac{\chi}{\chi^*}\right)}; \quad G(\chi) = 1 - \frac{\chi^*}{\chi}\mathrm{e}^{A\left(1-\frac{\chi}{\chi^*}\right)} \tag{3.19}$$

For a uniaxial tension process under monotonically increasing load, the temporal dissipation change is given by (3.6), with $\bar{\sigma} = n\sigma_t$ and

$$\overline{\Psi}_0 = \frac{1}{2}\varepsilon_t E^0 \varepsilon_t = \frac{(\sigma_t)^2}{2E^0} = \frac{\bar{\sigma}^2}{2n^2E^0}.$$

Integrating (3.6) in time we can calculate the total dissipated energy at the end of the uniaxial tension process as

$$\begin{aligned}\Xi_t^{\max} &= \int_{\bar{\sigma}^*}^{\infty}\frac{\bar{\sigma}^2}{2\rho_0 n^2 E^0}\frac{\mathrm{d}G(\bar{\sigma})}{\mathrm{d}\bar{\sigma}}\mathrm{d}\bar{\sigma} \\ &= \int_{\bar{\sigma}^*}^{\infty}\frac{\bar{\sigma}^2}{2\rho_0 n^2 E^0}\mathrm{d}G(\bar{\sigma})\end{aligned} \tag{3.20}$$

and after operating we get

$$\Xi_t^{\max} = \frac{(\bar{\sigma}^*)^2}{\rho_0 n^2 E^0}\left[\frac{1}{2} + \frac{1}{A}\right] \tag{3.21}$$

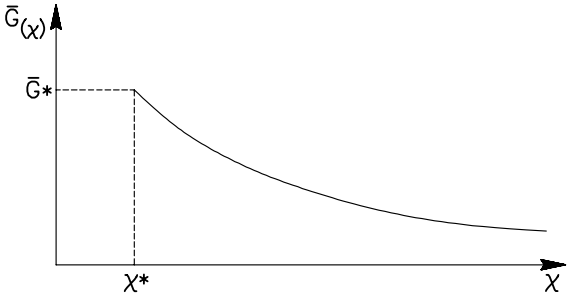

Fig. 5. Representation of function $G(\chi)$.

giving

$$A = \frac{1}{\dfrac{\Xi_t^{max}\rho_0 n^2 E^0}{(\bar{\sigma}^*)^2} - \dfrac{1}{2}} \tag{3.22}$$

where $\bar{\sigma}^*$ is the initial damage stress. Parameter A is never negative, as the material must dissipate at least the energy accumulated when reaching the initial damage stress $\bar{\sigma}^*$. Making the same hypotheses for a uniaxial compression process and postulating that parameter A must be the same in both cases, it is deduced that

$$A = \frac{1}{\dfrac{\Xi_c^{max}E^0}{(\bar{\sigma}^*)^2} - \dfrac{1}{2}} \tag{3.23}$$

and, as parameter A must be the same as in (3.22)

$$\Xi_c^{max} = n^2\Xi_t^{max} \tag{3.24}$$

The value of tension maximum dissipation Ξ_t^{max} is a material parameter equal to the fracture energy density g_f, parameter derived from fracture mechanics as $g_f = G_f/l_c$, where G_f is the fracture energy and l_c is the characteristic length of the fractured domain [26,30].

3.2.5. Tangent constitutive law

From (3.4), the variation of the stress tensor and finally the unsymmetric tangent constitutive tensor $\boldsymbol{C}^D$ of the damage model can be deduced as [6]

$$\delta\boldsymbol{\sigma} = \boldsymbol{C}^S\delta\varepsilon + \delta\boldsymbol{C}^S\varepsilon; \quad \delta\boldsymbol{C}^S = \frac{\partial\boldsymbol{C}^S}{\partial d}\delta d = -\boldsymbol{C}^0\delta d \tag{3.25}$$

$$\begin{aligned}\delta\boldsymbol{\sigma} = \boldsymbol{C}^D\delta\varepsilon &= \left[(1-d)\boldsymbol{I} - \frac{dG(\bar{\sigma})}{d\bar{\sigma}}\boldsymbol{\sigma}^0 \otimes \frac{\partial\bar{\sigma}}{\partial\boldsymbol{\sigma}^0}\right]\boldsymbol{C}^0\delta\varepsilon \\ &= (\boldsymbol{I}-\boldsymbol{H})\boldsymbol{C}^0\delta\varepsilon\end{aligned} \tag{3.26}$$

where

$$\boldsymbol{C}^D = (\boldsymbol{I}-\boldsymbol{H})\boldsymbol{C}^0$$

In these equations, $\boldsymbol{I}$ is the identity matrix of the same order as $\boldsymbol{C}^0$ and $\boldsymbol{H}$ is a nonsymmetric damage matrix, depending only on the stress vector $\boldsymbol{\sigma}^0$ of the undamaged material, as the damage variable is also implicitly related with the mentioned stress vector through the equivalent stress $\bar{\sigma}$.

3.3. Visco-elastic effects

The effect of damping on the material behaviour under dynamic loads is now considered by means of a Kelvin model. In this model, each point of the material undergoes the same deformation ε, so that the total stress $\boldsymbol{\sigma}_{tot}$ of the system will be the sum of a nonviscous stress $\boldsymbol{\sigma}$ and a viscous stress $\boldsymbol{\sigma}_{vis}$, i.e.

$$\boldsymbol{\sigma}_{tot} = \boldsymbol{\sigma} + \boldsymbol{\sigma}_{vis} = \boldsymbol{C}^S\varepsilon + \boldsymbol{\eta}^S\dot{\varepsilon} \tag{3.27}$$

where the secant viscous constitutive matrix $\boldsymbol{\eta}^S$ is defined here as

$$\boldsymbol{\eta}^S = \frac{\eta}{E^0}\boldsymbol{C}^S = \alpha\boldsymbol{C}^S \tag{3.28}$$

This viscous tensor definition is based on the hypothesis that at the end of the load process a material point remains completely relaxed, without stiffness nor cohesion between particles. For this reason, it is assumed in this work that the material point does not preserve its initial viscous characteristics and it loses viscosity proportionally with its loss of stiffness. However, this hypothesis is flexible and can be adapted to the material type without affecting the subsequent general formulation. In equation (3.28), η is the one-dimensional viscous parameter and α is the relaxation time, defined as the time needed by the elasto-viscous system to reach a stable configuration in the undamaged state.

With these assumptions, the behaviour of the system under virtual variations in strains and strain velocities can be obtained as

$$\begin{aligned}\delta\boldsymbol{\sigma}_{tot} &= \delta\boldsymbol{\sigma} + \delta\boldsymbol{\sigma}_{vis} = \boldsymbol{C}^D\delta\varepsilon + \alpha(\boldsymbol{C}^S\delta\dot{\varepsilon} + \delta\boldsymbol{C}^S\dot{\varepsilon}) \\ &= \boldsymbol{C}^D\delta\varepsilon + \alpha(\boldsymbol{C}^S\delta\dot{\varepsilon} - \boldsymbol{C}^0\dot{\varepsilon}\delta d)\end{aligned} \tag{3.29}$$

Introducing $\boldsymbol{\sigma}_{vis}^0 = \alpha\boldsymbol{C}^0\dot{\varepsilon}$ and using relation (3.26), the visco-elastic incremental strain–stress relation is obtained as

$$\begin{aligned}\delta\boldsymbol{\sigma}_{tot} &= \boldsymbol{C}_{vis}^D\delta\varepsilon + \alpha\boldsymbol{C}^S\delta\dot{\varepsilon} \\ &= (\boldsymbol{I}-\boldsymbol{H}_{vis})\boldsymbol{C}^0\delta\varepsilon + \alpha\boldsymbol{C}^S\delta\dot{\varepsilon}\end{aligned} \tag{3.30}$$

where $\boldsymbol{H}_{vis}$ takes the following value [6,7]:

$$\boldsymbol{H}_{vis} = d\boldsymbol{I} + \frac{dG(\bar{\sigma})}{d\bar{\sigma}}(\boldsymbol{\sigma}^0 + \boldsymbol{\sigma}_{vis}^0) \otimes \frac{\partial\bar{\sigma}^0}{\partial\boldsymbol{\sigma}} \tag{3.31}$$

4. Global damage indices

4.1. Basic concepts

The idea for the GDI definition stemmed from a macroscale analogy with the microscale local damage index (LDI) definition. Thus, the starting point for deducing a global structural damage index is Eq. (3.1), which defines local damage as a relation between the actual free energy Ψ of the damaged material and the elastic free energy Ψ_0 of a fictitious undamaged material. The latter energy corresponds to the specific strain energy the material would store should it undergo the actual strains while preserving its initial elastic properties. Therefore, the two above mentioned specific free energies may be mathematically interpreted as norms of

material stiffness, as the strain field is the same in both cases.

These considerations lead to the conclusion that the LDI is actually a coefficient that measures the loss of stiffness relative to the initial state at a particular physical location. A value of 0.2 for the LDI means that 20% of the initial stiffness at a material point has been lost during the nonlinear process.

4.2. Formulation

In the previous section the significance from a structural perspective of the LDI and the magnitudes involved in its definition was outlined. All this microscale philosophy is extensible to macroscale level in order to produce a GDI for a finite structural volume, containing an infinity of points, each with a different LDI.

It seemed natural to reach this objective by integrating the pointwise Eq. (3.1) over a finite mass, keeping in mind that $\mathrm{d}m = \rho_0 \mathrm{d}V$, as follows:

$$\Psi = (1-d)\Psi_0 \Rightarrow W_\mathrm{p} = \int_V \rho_0 \Psi \,\mathrm{d}V = \int_V (1-d)\rho_0 \Psi_0 \,\mathrm{d}V = (1-D)W_\mathrm{p}^0 \tag{4.1}$$

where D is the GDI of the considered structural mass, $W_\mathrm{p}^0 = \int_V \rho_0 \Psi_0 \,\mathrm{d}V$ is its fictitious ever-elastic potential energy due to the actual strains and W_p is the actual potential energy. Solving Eq. (4.1) for D, yields the final expression:

$$D = 1 - \frac{W_\mathrm{p}}{W_\mathrm{p}^0} = \frac{\int_V \rho_0 \Psi_0 \mathrm{d}V - \int_V (1-d)\rho_0 \Psi_0 \mathrm{d}V}{\int_V \rho_0 \Psi_0 \,\mathrm{d}V} = \frac{\int_V d\rho_0 \Psi_0 \,\mathrm{d}V}{\int_V \rho_0 \Psi_0 \,\mathrm{d}V} \tag{4.2}$$

This expression is formally similar to other proposed GDIs, usually sought as weighted volume averages of LDIs, but for the weighting factors ($\rho_0 \Psi_0$) that are particular to the proposed GDI.

In a finite element context, expression (4.2) takes the following operational form:

$$D = 1 - \frac{\sum_e \boldsymbol{a}^\mathrm{T} \int_{V^{(e)}} \boldsymbol{B}^\mathrm{T} \boldsymbol{\sigma} \mathrm{d}V}{\sum_e \boldsymbol{a}^\mathrm{T} \int_{V^{(e)}} \boldsymbol{B}^\mathrm{T} \boldsymbol{\sigma}^0 \,\mathrm{d}V} \tag{4.3}$$

where $\sum_e$ denotes the sum over a number of finite elements, $\boldsymbol{a}$ is the mesh nodal displacement vector, $\boldsymbol{B}$ is the strain displacement matrix, $V^{(e)}$ is the volume of each finite element (e), $\boldsymbol{\sigma}$ is the actual stress vector and $\boldsymbol{\sigma}^0$ is the stress vector should the material preserve its original characteristics and undergo the actual strains. The sum is performed over the group of elements for which a value for the GDI is sought. It may be observed that the smallest entity on which a GDI may be calculated is a single finite element.

4.3. Properties

Expression (4.3) of the GDI depends exclusively on the actual nonlinear stresses and the hypothetically linear ones. It is absolutely general in the sense that it is independent of the local constitutive model. The local damage model described in this paper served as theoretical basis for deducing the GDI methodology, but is not at all a compelling requirement for its application. However, the objectivity and accuracy of the GDIs will always depend on those same qualities of the local model. This is so because the GDI methodology does not have the least effect on structural behaviour as it is basically a tool for assessing the state of a structure. It is not responsible for the manner the structure has reached its actual configuration. Thus, the GDI evaluation methodology operates as a postprocess that may be implemented with relative ease in any existing nonlinear finite element code.

A GDI value has the significance of the unit complement of the ratio between the potential energy of the actual strain field the structure undertakes because of damage and the hypothetic potential energy the structure would store had it stayed undamaged under the same strain field. Furthermore, the GDIs, similarly to the LDIs, give a measure of structural stiffness loss.

All these considerations seem to lead to the conclusion that both LDIs and GDIs share similar nature and properties. Nevertheless, there is a most important and enlightening difference not apparent at first view, that needs special emphasis. While Eq. (3.5) clearly states the nondecreasing nature of LDIs, therefore the irreversibility of local damage, an equivalent statement for GDIs is not possible, meaning GDIs may indeed decrease in special circumstances. The explanation of this intriguing characteristic lies in the integral nature of GDIs in contrast with the material intrinsic nature of LDIs.

An example will bring a clearer understanding of the phenomenon: Imagine a four-legged chair with one leg considerably weaker that the other three. Suppose that somebody rests his substantial weight on that frail leg braking it. Now the chair will be unable to bear even the lightest child sitting on the chair exactly in the same way as when it was led to failure. This situation clearly corresponds to a GDI for the entire chair of 1, LDIs of 1 somewhere along the broken leg and no local damage for the remainder legs. Now suppose further that the same light child sits on the leg opposite the broken one and that leg withstands the small load within the elastic behaviour range. The GDI for the entire chair in his new circumstance is definitely 0, as there is no difference between the behaviour of the broken chair and that of an identical new chair. Why? Because the broken leg

plays no role anymore, the chair is bearing the new load without needing its strength.

This behaviour highlights the filtering characteristic of GDIs, consisting in eliminating the contribution of irrelevant parts of the structure and identifying and following the evolution of its critical zones. The responsibility for this feature lies with the strain field acting as weighting factor in the GDI definition. This selects only those structural parts whose contributions to the capacity to resist the applied load, are significant.

The above example stresses the obvious fact that the damage level depends strongly on the applied load. The immediate consequence is that GDIs are measures of stiffness vis-à-vis the loads causing the damage. In case of proportional loads (fixed loads that vary proportionally only in amplitude), the GDIs are as irreversible as the LDIs. If the load characteristics change, such as in dynamic analyses, the GDIs may oscillate as the various load-bearing capacities are brought in and out of action, while LDIs always stay irreversible.

All this renders impossible the general description of structural state exclusively by means of GDIs, disregarding the load that induced the damage. However, in most cases there is a nonzero damage correlation level between the various loads acting on a structure. For example, the damage generated by an earthquake (horizontal loads) generally affects the structural behaviour under service loads (vertical loads), but almost never the damage level is transmitted entirely, signifying that the GDIs are not the same when the type of load changes.

The inconvenience arising from the nonirreversible nature of GDIs may be circumvented if a reference load, such as dead-load or service load, is established for comparison purposes. This implies unloading the damaged structure and subsequently reloading it with the reference load. This unifying criterion allows obtaining comparable GDIs for different loads.

These properties of the GDI allow the study of the evolution of structural load-carrying capacity along complex load histories. The GDI always shows synthetically the quota of initial structural resistance that has been lost due to the nonlinear behaviour of constitutive materials under a certain load.

5. 3D Reinforced concrete finite element

The 20-node tri-quadratic isoparametric hexahedrical serendipity element is used for computations in this work. The stiffness and mass matrices are derived in the usual way as

$$\boldsymbol{K}_{\mathrm{c}} = \int_V \boldsymbol{B}^{\mathrm{T}} \boldsymbol{C}_{\mathrm{c}} \boldsymbol{B}\,\mathrm{d}V, \quad \boldsymbol{M} = \int_V \boldsymbol{N}^{\mathrm{T}} \rho \boldsymbol{N}\,\mathrm{d}V \tag{5.1}$$

where $\boldsymbol{B}$ is the strain–displacement matrix, $\boldsymbol{C}_{\mathrm{c}}$ is the material constitutive matrix for concrete and the integral

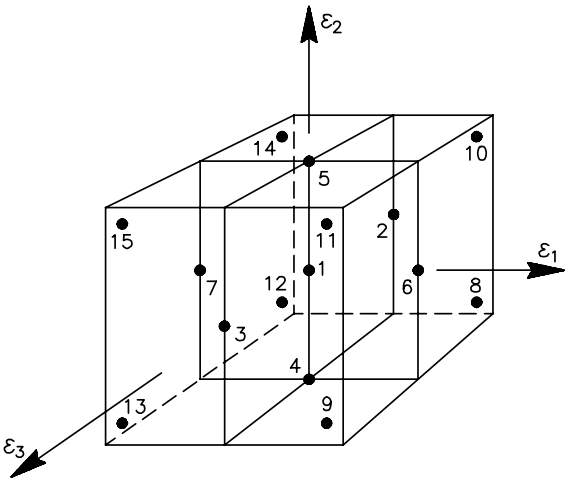

Fig. 6. Integration points distribution for the hexahedrical element.

extends over the volume of the element. The numerical integration is performed using a reduced quadrature of 15 integration points instead of the usual $3 \times 3 \times 3$ point Gaussian quadrature, without losing accuracy and efficiency [9,34]. The rule is (see Fig. 6)

$$\begin{aligned} &\int\int\int_{-1}^{+1} f(\epsilon_1, \epsilon_2, \epsilon_3)\,\mathrm{d}\epsilon_1\,\mathrm{d}\epsilon_2\,\mathrm{d}\epsilon_3 \\ &\quad = Af(0,0,0) + B[f(-b,0,0) + f(b,0,0) + \cdots] \\ &\qquad + C[f(-c,-c,-c) + f(-c,-c,c) + \cdots] \end{aligned} \tag{5.2}$$

where ϵ_1, ϵ_2 and ϵ_3 are the normalised natural coordinates. The weight factors and the sampling points take the following values: $A = 1.564444$, $B = 0.3555556$, $C = 0.5377778$, $b = 1.000000$ and $c = 0.6741000$. The position of these sampling points includes six points on the centre of the faces and one point in the centre of the element.

Perfect bond between the reinforcement bars and the surrounding concrete is assumed. This displacement compatibility allows treating the steel as integrant part of the 3D finite element. The steel stiffness matrices of all layers $\boldsymbol{K}_{\mathrm{s}}^{i}$ are added to that of the concrete, $\boldsymbol{K}_{\mathrm{c}}$, thus obtaining the total stiffness (see Fig. 7) as

$$\boldsymbol{K} = \boldsymbol{K}_{\mathrm{c}} + \sum_i \boldsymbol{K}_{\mathrm{s}}^{i} \tag{5.3}$$

Each set of reinforcement bars is distributed as a bidimensional layer of equivalent thickness placed within the concrete element in a position such that one of the local natural coordinates is constant for that layer. In that plane, the stiffness of the layer is oriented according to the direction of the actual bars.

The stiffness contribution of each steel layer is computed as follows:

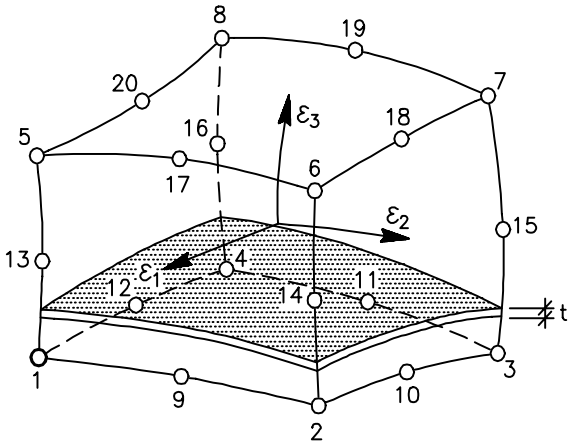

Fig. 7. Concrete 3D element with a reinforcement steel layer.

$$\boldsymbol{K}_{\mathrm{s}}^{i} = \int\int_{\Omega^i} \boldsymbol{T}^{\mathrm{T}}\boldsymbol{B}^{\mathrm{T}}\boldsymbol{C}_{\mathrm{s}}^{i}\boldsymbol{B}\boldsymbol{T}t\,\mathrm{d}\Omega \tag{5.4}$$

where $\boldsymbol{C}_{\mathrm{s}}^{i}$ is the constitutive matrix of the steel layer i, $\boldsymbol{T}$ is the rotation matrix from the local coordinate system attached to the steel bar to the global coordinate system, t is the equivalent thickness of the layer and the integral is performed over the surface of the layer Ω^i.

The described element admits any number of layers, each made of a different material and with either uniaxial or biaxial behaviour. In this study, the reinforcement bars are assigned unidirectional stiffness properties. Their constitutive behaviour is modelled by means of an elasto-plastic hardening law with elastic unloading. A strain limit corresponding to sudden failure is also considered.

6. Plane frame failure simulation

A simple plane frame constitutes a good test case in this exercise meant to display the possibilities the new GDI methodology opens for the assessment of the damage history of entire structures and its component parts. It will be shown how the GDI methodology may be used to deepen the understanding of intimate localised failure mechanisms and load redistributions within a civil engineering structure.

The frame is subjected to a static load and the properties of the GDIs will be easily highlighted as the intuitive character of structural behaviour will render them evident.

6.1. Structural description

A layered Timoshenko quadratic beam finite element [18] was used in the study of the frame in Fig. 8 subjected in its left upper corner to the static action of an imposed horizontal incremental displacement up to 4% of total hight (push-over test). The RC frame is 9 m high and 6 m wide and has three floors.

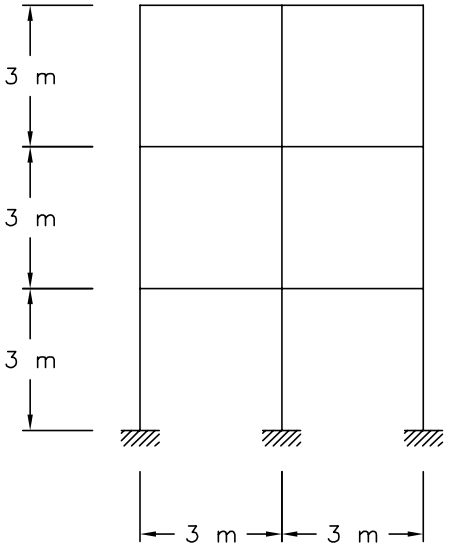

Fig. 8. Studied frame geometry.

The columns have 30×30 cm cross-sections reinforced symmetrically with 4.35% steel and the beams 40×30 with 5.3% steel. These reinforcement percentages are unrealistic and were chosen so high for demonstration purposes. All finite elements are 1 m long and have 20 layers, the 2nd and the 19th of steel and the remainder of concrete. Typical material properties are assumed for both materials. The constitutive model for concrete is the isotropic damage model described in Section 3, while for steel a perfect elasto-plastic law was chosen, such that, once the steel reaches the elastic limit, it yields indefinitely at constant stress.

6.2. Results

The plane frame was analysed with the GDI methodology during all the load history. The purpose was to monitor how the GDIs describe the shifting patterns generated by stress redistribution due to damage and their capacity to discern the relevant parts of the structure that play a key role in its behaviour.

In order to compare the behaviour of the critical parts of the structure, seven nondisjunctive sets of finite elements have been observed during the load process: the whole structure, the three floors comprising each three columns plus their two upper beams and, finally, the three columns of the first floor separately.

The evolution of the resistant force versus the displacement imposed in the left upper corner of the frame

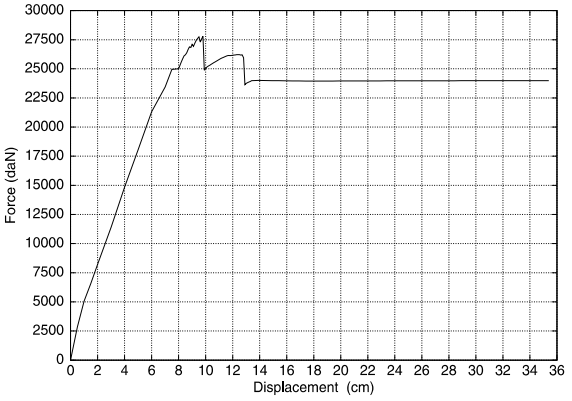

Fig. 9. Force–displacement curve for the left upper corner.

are presented in Fig. 9. The evolution of GDIs for the entire frame and the three floors are shown in Fig. 10. Studying together these two graphs may be observed that there are two sudden reductions of the force response corresponding to sudden increases of the total GDI and that of the first floor, and, to a lower extent, of the other two floors. The explanation is found in the detailed damage history of the first floor depicted in Fig. 11.

It is clearly expected that the structure will fail through weakening of the columns of the first floor, first the leftmost as it undergoes severe tension coupled with the ground level bending, second the middle column ceases to function and last the right column. It is therefore clear that these three columns, belonging to the first floor, constitute the critical parts from the point of view of the capacity of the frame to withstand the external load. This phenomenon is perfectly captured by their GDIs (Fig. 11) so that towards the end of the loading history all three columns share the same level of damage. It may be noted that the GDI of the first floor is always an average of the GDIs of its three columns even though it also comprises two beams but they add practically nothing to the first floor GDI.

When the entire structure GDI evolution is compared with those of the three floors (Fig. 10) the whole damage process gets clearer. The overall GDI and floors GDIs behave similarly until the brittle collapse of the third column of the first floor, which occurs for an imposed displacement of around 10 cm (Fig. 11). From that point on (after the first dramatic decline in response force—Fig. 9) the overall GDI assumes more and more completely the behaviour of the first floor, ignoring what happens to the rest. It seems that at this point the overall GDI decided that only the first floor state is relevant and this idea seems to be maintained until the end of the load history.

The second steep fall in response force at 13 cm imposed displacement (Fig. 9) corresponds to the brittle failure of the first floor columns concrete in compression, and the ensuing redistribution of stresses towards the steel. It corresponds to a change of static configuration for the whole structure due to the formation of perfect plastic hinges and not to important changes of damage levels. Starting at that point, the concrete is practically inexistent at hinge locations and only the steel remain there so that the response force stays constant as the steel has a perfect plastic behaviour from here on.

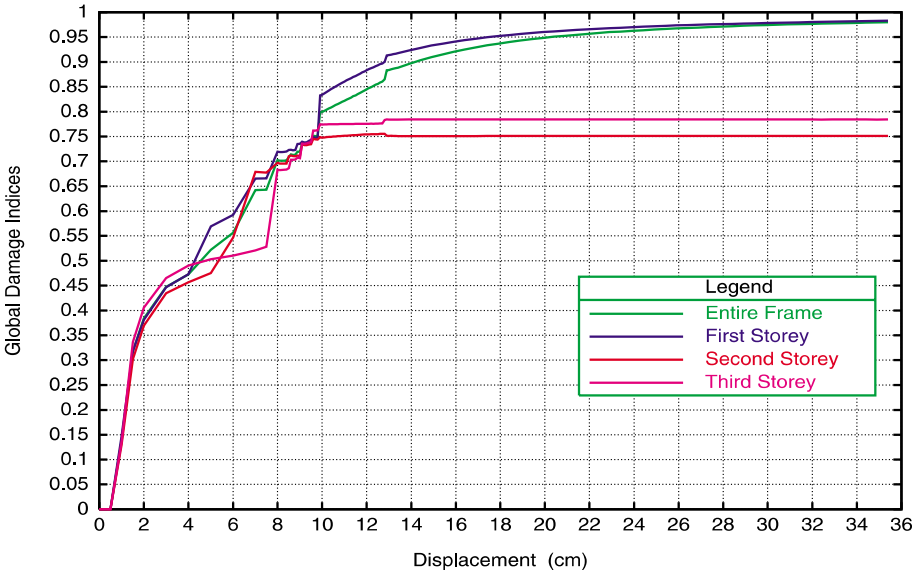

Fig. 10. Evolution of the GDIs for the entire frame and its three floors.

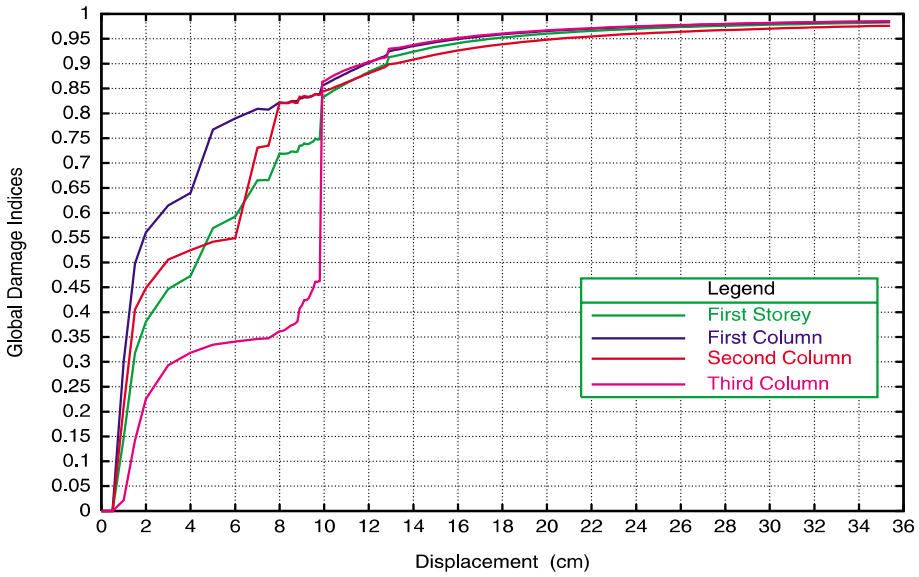

Fig. 11. Evolution of the GDIs for the first floor and its three columns.

Fig. 12 presents the deformed shapes with the correspondent elemental GDIs (GDIs for each finite element separately) distributions for imposed displacements of 9.2 cm, before failure of the third column (Fig. 12(a) and (b)), and 35.5 cm, close to failure (Fig. 12(c) and (d)) respectively. The mentioned change in static configuration may be observed as well as the relatively even damage distribution before plastic hinge formation at the ends of first floor columns, where damage levels are maximum at the end of the load history.

7. Pathology of a housing building

Housing buildings often display structural problems after completion when, due to constructive vices, exceptional loads like earthquakes or later accidents like ground movements, these are rendered unserviceable and rehabilitation decisions need be taken.

The methodology described herein proposes reconstructing through numerical analysis the surveyed damaged state of a structure and in this manner explain the underlying reasons of unaccounted-for structural behaviour while simultaneously quantifying them by means of GDIs. These indices signal the weaker zones and provide the measure of their experimented stiffness loss. When a configuration similar to the real state of the building is found, deductions can be made about the actual structural characteristics using similarity techniques.

Numerical simulations carried out with the damage model can provide assessments of the proposed repair works and help define the optimum intervention, being a valuable tool both for diagnosis and rehabilitation of buildings.

7.1. Description of the structure

The studied structure is a five-storey building with two symmetrical flats per floor. The third floor presented extensive damage from unknown reasons and was therefore the object of detailed analysis. The finite element mesh and the RC members of the semi-structure actually analysed are shown in Fig. 13. This study was performed using the 3D RC finite element described in Section 5.

The trouble with this building was that soon after completion and being already in use, micro-cracks which soon became important cracks appeared. That fact imposed urgent measures which were developed in two stages: survey of the actual state of the building and numerical modelling in order to simulate its behaviour.

7.2. Strategy of analysis

The applied load in the numerical simulation consisted in own weight plus an incremental pressure on both upper and lower floors so scaled so that nominal service load correspond to a load factor of 1.

Fig. 14 shows the cracks observed on the third floor during the survey and those same cracks as obtained from the analysis results. The most important cracks were detected in the partition walls and excellent overall correlation with the analysis was accomplished, with exactly the same localisations as in the real case, but for

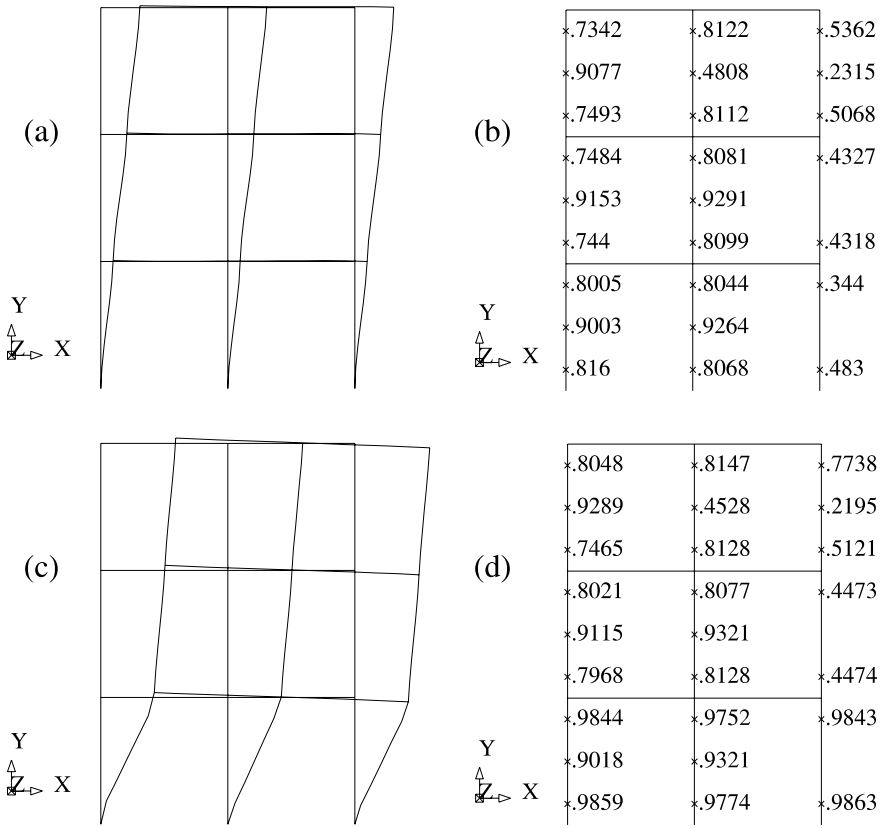

Fig. 12. Deformed shape and elemental GDIs for two characteristic moments of the load history.

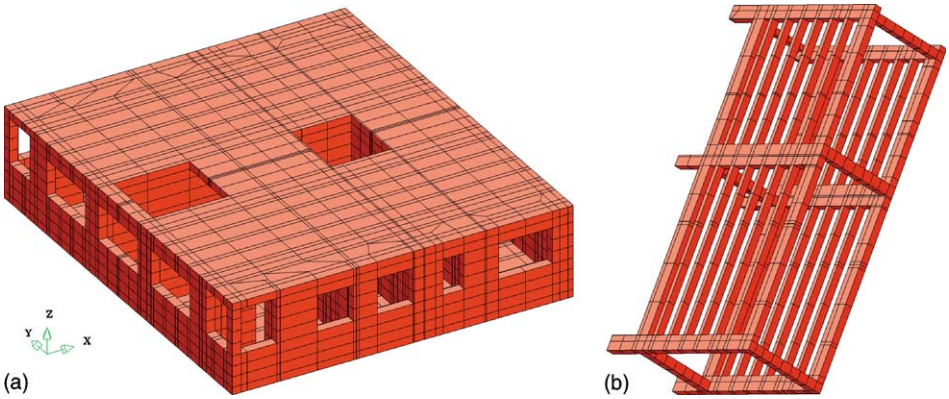

Fig. 13. Third floor mesh. Reinforcement bearing members of half structure.

a load factor of 4. This suggests that the trussed joists in the floors are much more flexible than expected given that the partition walls are not supported by any column. However, as complete failure occurred for a load factor of 5.9, may be concluded that the actual safety factor is only 1.45 and that the actual state of the structure under service load is that corresponding to the computed configuration subjected to 4 times the service load.

In view of this surprising result, a verification campaign was initiated and it was discovered that the reinforcement bars of trussed joists and some of the beams

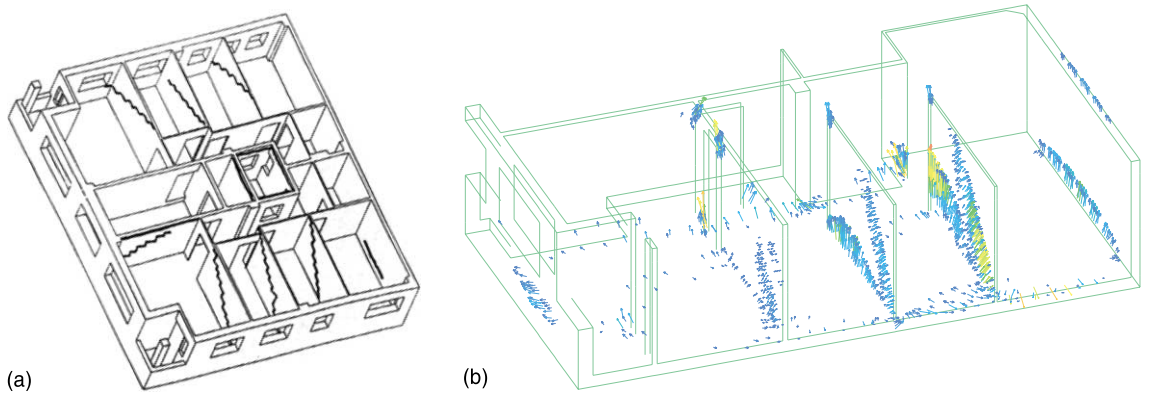

Fig. 14. Third floor cracks: (a) visual survey and (b) numerical simulation.

showed important drift from design specifications about distance between bars that leads to important stiffness alterations.

Fig. 15 shows elemental damage distribution and confirms that the cracks appear in the most damaged zones. Fig. 16 presents the evolution of GDIs for the complete floor and its constitutive parts. The dominant GDI is that of the partition walls as the overall GDI traces its trajectory since the beginning of the load history. The second most decisive GDI is that corresponding to the beam filling.

This paramount role of plain masonry parts suggests that the intended resistant members are failing their mission. The message that this anomalous behaviour sends is that the serviceability of the structure depends on structural parts which are not supposed to play this role. Thus the GDI is proven to be a resourceful tool for structural health assessment.

8. Failure pressure evaluation of the containment building of a large dry nuclear power plant

The evaluation of the failure pressure of the containment building of a large dry PWR-W three loops nuclear power plant is described in this section. The method considers fully tridimensional finite element models in order to take into account the effect of the most significant structural characteristics (presence of three buttresses, penetrations, additional reinforcement around the penetrations, etc.), the lack of symmetry of the forces generated by the prestressing system, as well as the nonlinear behaviour of the materials and the sensitivity of the results to uncertainties associated with several material parameters.

The GDI methodology is used to ascertain the influence of structural parts on the overall structural behaviour and to identify and confirm the causes of failure.

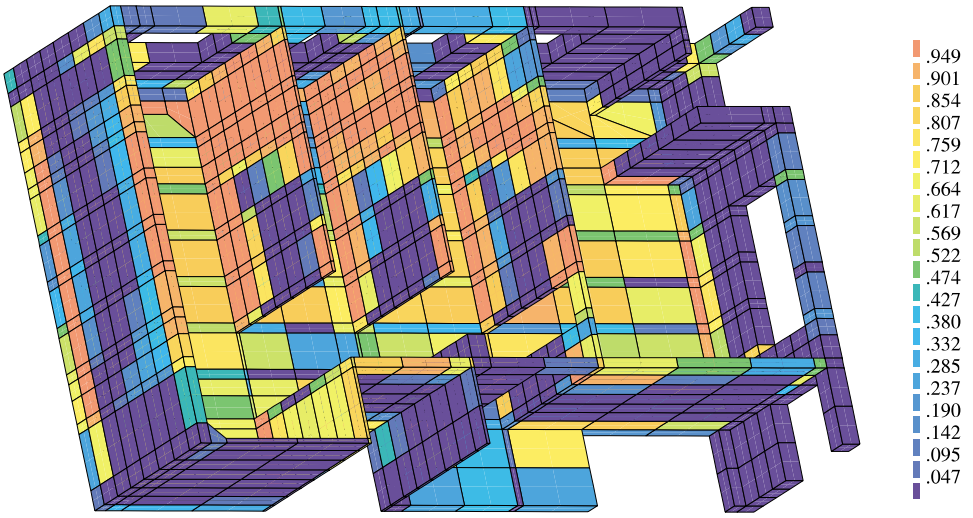

Fig. 15. Elemental GDIs map at failure.

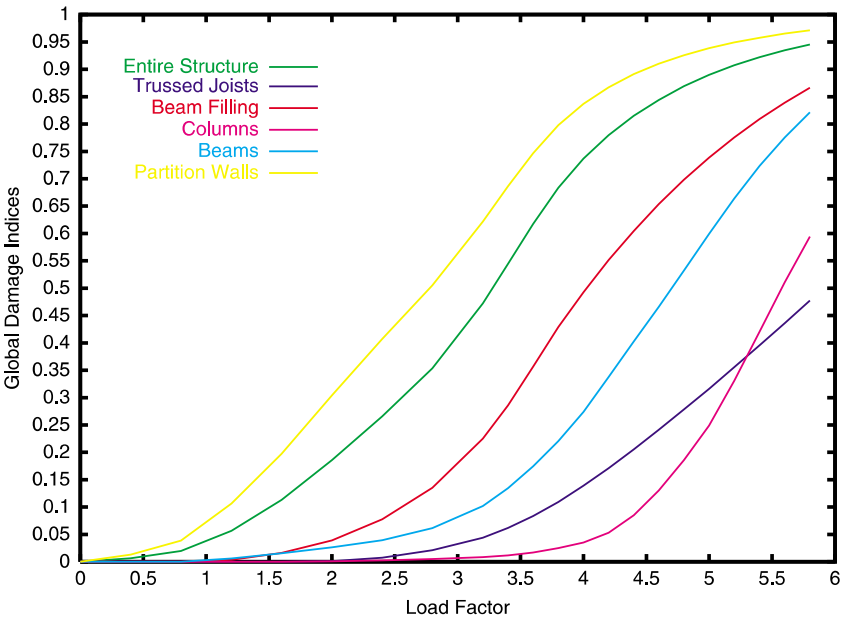

Fig. 16. Global damage indices evolution.

8.1. Description of the structure

The RC containment building which hosts the reactor core and its cooling system consists of a massive foundation slab and a vertical cylindrical wall closed on the upper part by a hemispherical dome. The structure has an additional prestressing system for the wall and the dome consisting of nonadherent tendons and its interior is protected with a steel liner having a sealing role. Fig. 17 shows vertical and horizontal cross-sections of the structure, including the main geometrical parameters. The most important dimensions of the structure are: interior diameter of the wall 40 m, interior total height 63.4 m, interior height of the cylinder 43.4 m, thickness of the foundation slab 3 m, thickness of the cylindrical wall 1.15 m, thickness of the dome at its highest point 0.95 m, average liner thickness 6.5 mm.

There are three vertical buttresses on the outer side of the cylindrical wall spaced at 120°, which serve as support for the horizontal prestressing system. The penetrations in the cylindrical walls having a major impact (being modelled therefore) on the structural behaviour are: the personnel airlock, the equipment hatch, the emergency airlock, the main steam penetration, the fuel transfer penetration and the purge line penetration.

The prestressing system is also shown in Fig. 17. There are 132 horizontal tendons, comprising an angle of 240° each, anchored in the 3 buttresses and 80 vertical tendons in 2 families (N–S, E–W) anchored in a perimetrical gallery located in the lower part of the foundation slab.

8.2. Strategy of analysis

The failure pressure is defined as the inner pressure corresponding to the structural material exhaustion, that is, to a certain strain limit of the reinforcement steel, prestressing tendons and liner. The failure criterion assumes that local steel rupture occurs when the mentioned strain limit reaches 0.8% for the reinforcement and 1% for the tendons. The straining up to failure limit of the reinforcement is made possible by the damage-induced stress loss in concrete leading to stress redistribution towards the steel components. The global damage indices describe the state of entire structural parts, summing up both concrete and steel data.

The loads considered in the analysis were the self-weight, the external pressures generated by the prestressing system and the internal pressure corresponding to a specified accident. The distribution of the pressures equivalent to those produced by the prestressing system has been evaluated analytically for all the nodes of the mesh. All the possible sources of prestressing losses have been included in this evaluation, i.e. friction, wobble, anchor set, instantaneous and long term, etc. The internal pressure was incremented gradually until the structural collapse occurred.

The model was calibrated using actual displacement and outside temperature measurements obtained during a 4-day real pressurisation experiment performed at the studied nuclear power plant. During the test, the inner pressure was increased up to 1.15 times the design pressure, which was 0.372 MPa. The results of the

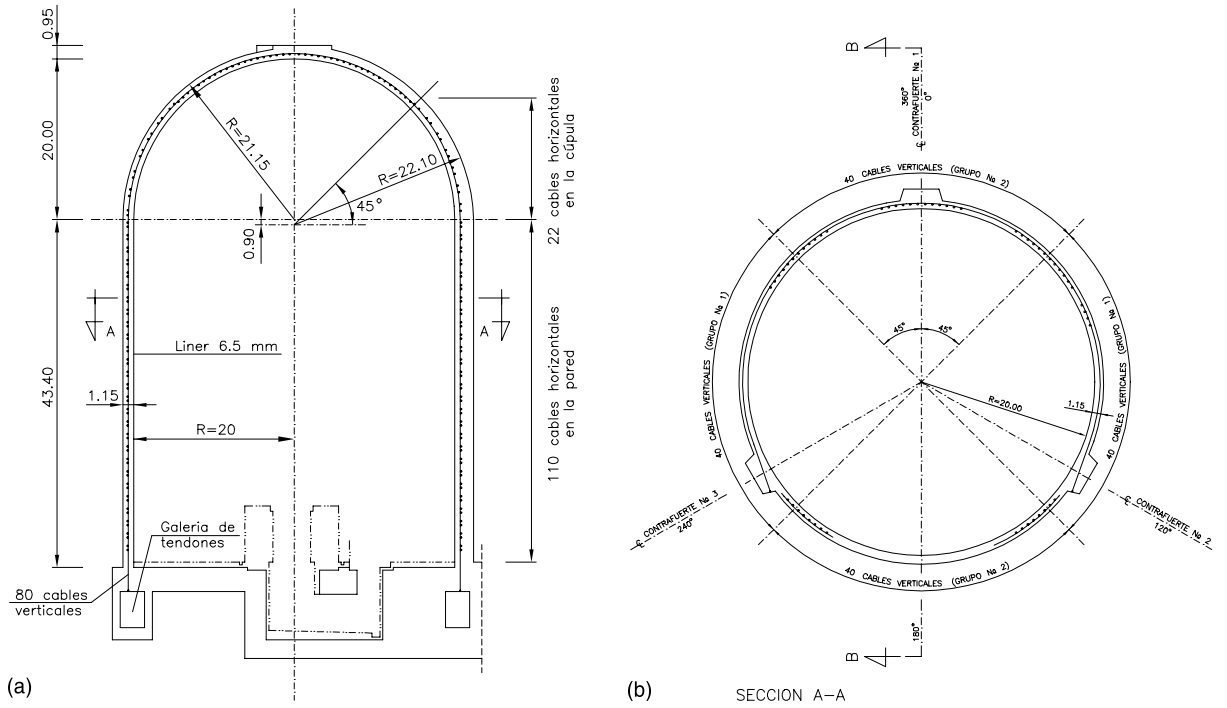

Fig. 17. Containment shell: (a) vertical section and (b) horizontal section.

mentioned test allowed to calibrate those parameters of the model referring to the amount of reinforcement steel to be included in the regions were unconsidered penetrations exist. It was a safe way to determine how much of the actual reinforcement is needed to counter the loss of wall stiffness due to the penetrations.

8.3. Failure pressure evaluation

The influence of including the foundation slab in the structural model on the global structural behaviour and especially on the failure pressure was first examined. The results show that the influence of including the slab is quite small for low levels of internal pressure; it decreases further as the pressure increases and it is negligible near the failure pressure, which is 1.11 MPa in both cases. This gives a safety coefficient of the structure related to the design pressure of 2.78. Furthermore, the cylindrical wall behaves better when the slab is present, due to the fact that the displacements of the slab slightly reduce the circumferential displacements of the wall; this allows to conclude that by not including the slab, one stays on the safety side during the complete load history. The comparison was based on an extensive survey of displacements, cracking patterns and reinforcement stresses along the load path.

A comparison was made of the radial displacement–pressure curves for the models with and without foundation slab, corresponding to the same point of the structure at the cylinder mid-height, where maximum displacement occurs. Slightly different responses were obtained for pressures over 0.7 MPa, due to the fact that cracking appears at the slab-wall junction, thus softening the wall clamping effect in the model which includes the slab. This difference does not affect the failure pressure, and changes only slightly the displacements at failure.

Fig. 18 shows results of a typical simulation of the behaviour of the structure under increasing internal pressure until failure. Fig. 18(a) shows a map of elemental damage of the structure, while Fig. 18(b) shows the broken reinforcement bars at the moment of failure, corresponding to strains higher than 0.8%.

The model used in the analysis demonstrates an important capacity of localising the deformation when the damage sets in. Once cracking diminishes the stiffness of concrete, the reinforcement remains the only element to withstand the pressure. This reduces heavily the impact of the concrete and therefore of its constitutive behaviour on the failure pressure of the containment and suggests that its complexity may be kept at a minimum.

Fig. 19 presents the evolution of several GDIs belonging to the most representative (from a failure pressure viewpoint) zones of the structure. Given that the failure occurs at mid-cylinder, the cylinder was divided in three disjoint rings of finite elements: the first ring is made of the lower row of elements that join the slab, the second ring contains the following three rows and the

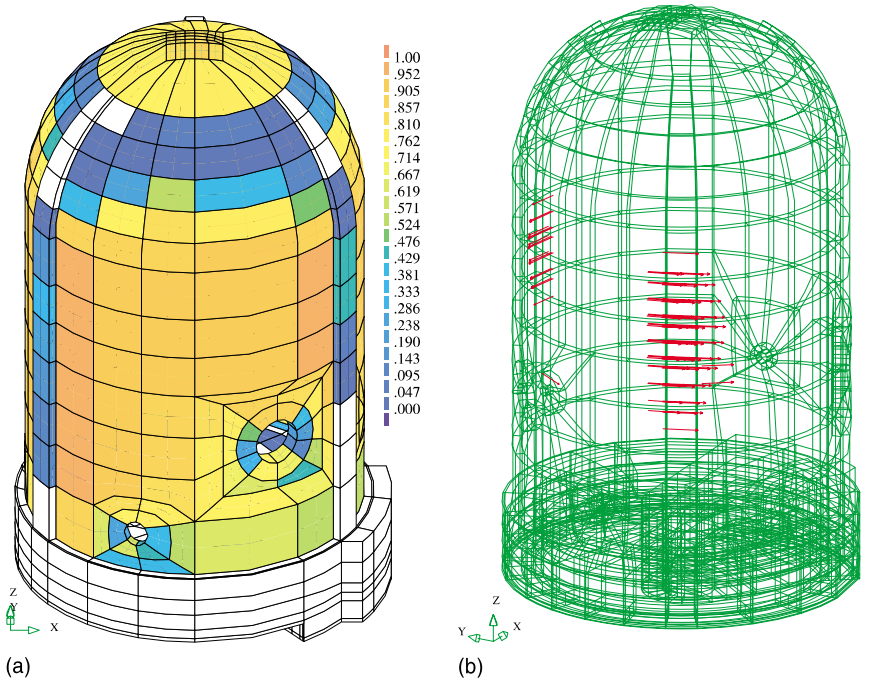

Fig. 18. Structural failure: (a) damage distribution and (b) broken steel bars.

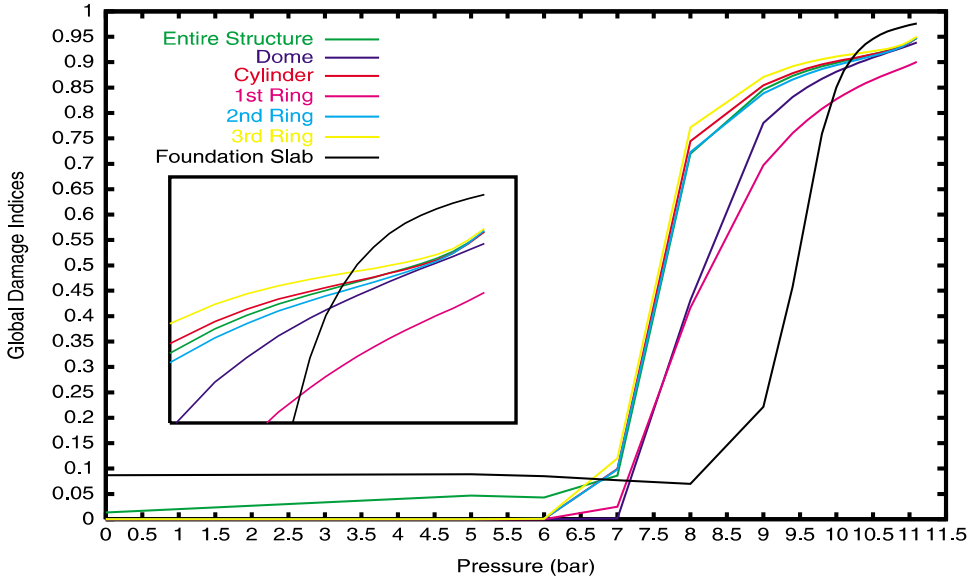

Fig. 19. Model with slab: global damage indices evolution.

last three rows that end where the dome begins belong to the third ring. Separately, GDIs for the cylinder as a whole, the dome, the slab and the entire structure were also calculated. Zooms of the final instants are shown in a box in the graph, in order to observe in detail what happens just before failure.

The first observation is that the presence of the foundation slab does not influence in the overall degradation patterns which develop at mid-cylinder. The overall GDI and the GDIs for cylinder, the second and third rings take very close values, which means that the overall damage takes into account exclusively what

happens in those rings, and that what happens with the rest of the structure has little relevance. Moreover, although the slab GDI displays important variations and finally takes values well above the overall GDI, the latter is never influenced by the state of the slab and the driving influence keeps being that of the above-mentioned rings. Also, the states of the first ring or the dome have little effect, while the cylinder GDI at his turn behaves like the overall GDI. The fact that the overall GDI reaches in both cases values close to the unit show that the structure really fails when the pressure reaches 11.1 bars.

In the segments close to the failure pressure (see box) it may be seen that the total, cylindrical wall and rings two and three GDIs get ever closer and their curves change curvature, sign that the reinforcement started to fail in those rings. Although the broken reinforcement bars are extremely localised, it may be observed that the overall GDI captures the phenomenon in all its intensity.

Seismic analyses of the containment building were also performed. The Californian 1940 El Centro earthquake was selected as reference seism, the effect on the structure of several intensity amplitudes being studied. The results showed that the building resists an El Centro type earthquake at 20% real amplitudes of the ground accelerations which corresponds roughly to seismic regulations-stipulated maximum ground acceleration at the real location site. For higher intensities, the structure collapses due to failure of vertical reinforcement at the base of the cylindrical wall, that suffers large stresses while the building swings during the earthquake.

Fig. 20 presents the distribution of elemental GDIs after the 20% intensity earthquake. It confirms the expected behaviour consisting in severe degradation of the lower ring (first ring) of finite elements as the reinforcement bars experience severe strains leading to widespread yielding of the steel (Fig. 21). Fig. 22 displays the evolution of significant structural parts throughout the duration of the seism. Although less than 3% of total structural volume undergoes important damage levels (Fig. 20), the overall GDI consequently reaches values above 70%. This behaviour of the GDIs highlights its property to correctly assess structural fitness vis-à-vis the applied load. Moreover, the observation of the behaviour of the rest of the GDIs can be enlightening to the intimate understanding of the structural response under these loading circumstances. Thus, in Fig. 23 can be seen that the first ring is the most damaged (90%), the second ring is slightly damaged (30%) and the third ring together with the Dome are almost as new. The cylinder as a whole, comprising all three rings, reaches values of GDI approximately 5% higher than the overall GDI but 15% lower than first ring. These data certifies that the structure as a whole is not at collapsing stage, as the influence of the first ring,

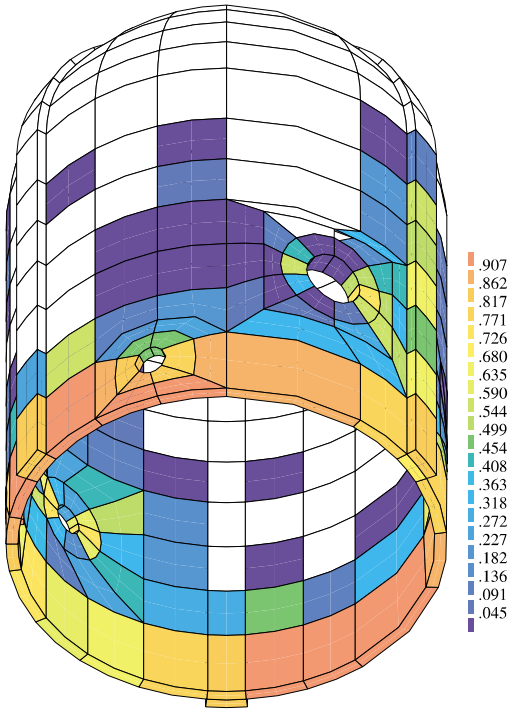

Fig. 20. Elemental GDIs after El Centro earthquake at 20% intensity.

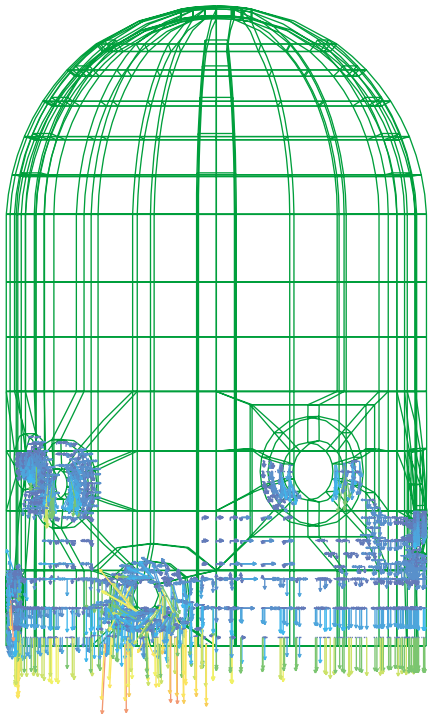

Fig. 21. Reinforcement bars surpassing yield limit during the 20% intensity seism.

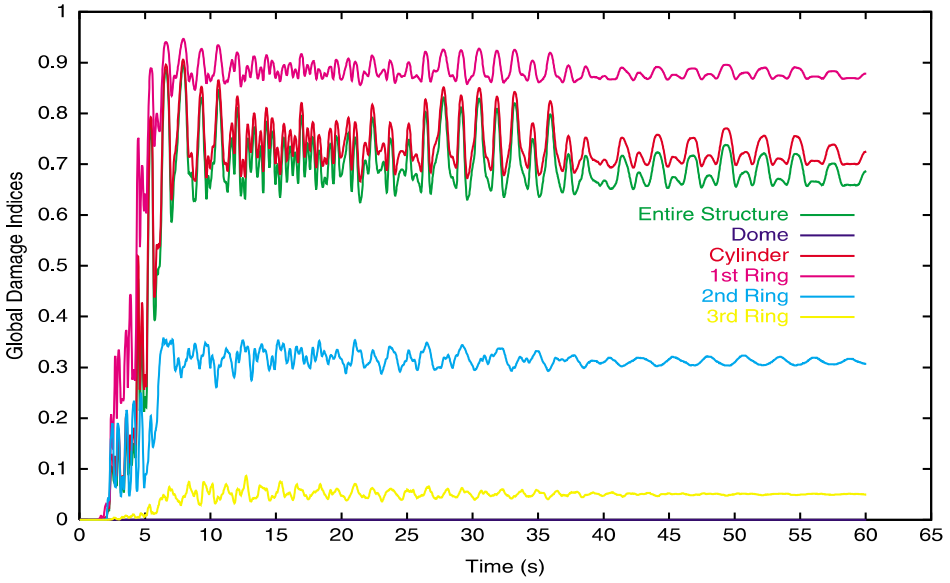

Fig. 22. Global Damage Indices evolution for El Centro earthquake at 20% intensity.

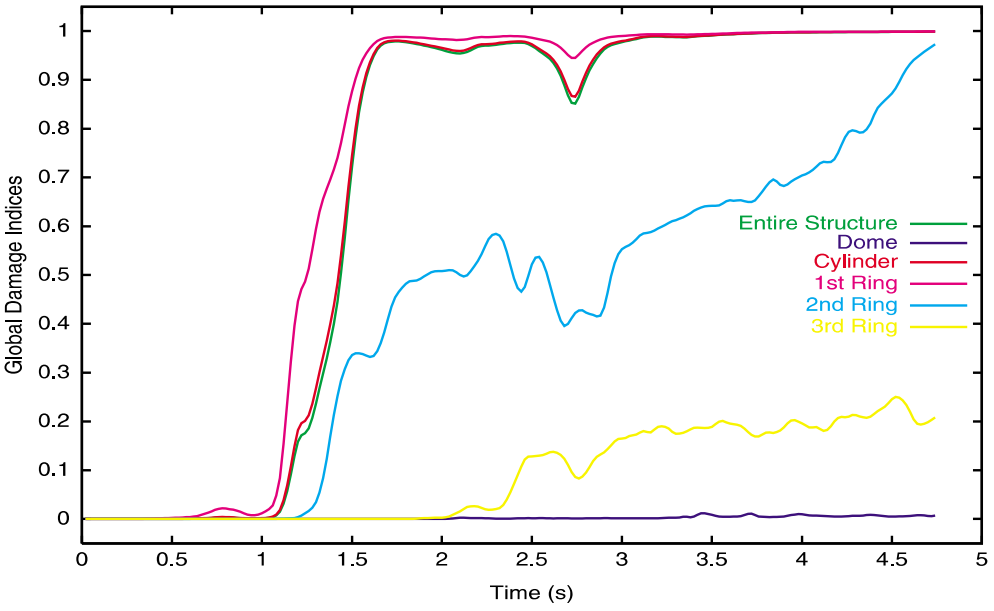

Fig. 23. Global damage indices evolution for El Centro earthquake at 100% intensity.

although dominant, is not overwhelming. It that were not true, the GDI levels of the first ring would be transfered in totality to its hierarchically superior structural subsets that are, in order, the cylinder and the whole structure. As it is, the undamaged zones of the structure still preserve a certain specific weight in the overall GDI, showing that the building is not close to collapse and still retains some loading capacity.

The opposite situation occurs when the El Centro earthquake strikes at full power (Fig. 23). In this case the overall GDI tracks closely from the very beginning the GDI corresponding to the cylinder that is strongly influenced by the first ring. That the overall GDI sticks to cylinder GDI shows how it forecasts the structural collapse and its cause almost from the start of the loading history. Structural failure occurs very quickly after only

4.75 seconds due to the complete braking of vertical reinforcement bars. All three mentioned GDIs reach levels of 100% signalling failure of the corresponding structural parts to resist the acting load.

Further details about this study may be found in [8].

9. General conclusions

A new numerical global damage evaluation method developed on a sound energy formulation base was presented.

The GDI was proved to be a powerful and precise tool for identifying the failure load and structural mechanisms leading to failure of RC structures.

The GDI provides accurate quantitative data on the state of any component subpart of a damaged structure and its importance to the overall structural behaviour, being of invaluable help to the task of assessing the reliability, safety and health of a structure and may well assist in the definition of adequate repair or retrofitting strategies.

Examples illustrating all facets and characteristics of the GDI methodology were provided.

References

[1] Arrea M, Ingraffea AR. Mixed mode crack propagation in mortar and concrete, Department of Structural Engineering, Cornell University, Report 81-13, Ithaca, New York, 1981.
[2] ASCE. Committee on Concrete and Masonry Structures, Task Committee on Finite Element Analysis of Reinforced Concrete Structures: A State-of-the-Art Report on Finite Element Analysis of Reinforced Concrete Structures, ASCE Spec. Pub, 1981.
[3] Bažant Z. Mechanics of distributed cracking. Appl Mech Rev 1986;39:676–705.
[4] Banon H, Biggs JM, Irvine HM. Seismic damage in reinforced concrete frames. J Struct Div, ASCE 1981;107(ST9): 1713–29.
[5] Barbat AH, Oller S, Oñate E, Hanganu A. Simulation of damage phenomena in required concrete buildings subjected to seismic actions. In: Alder H et al., editors. Numerical methods in engineering and applied sciences. Barcelona: CIMNE; 1992.
[6] Barbat AH, Hanganu A, Oller S, Oñate E. Rigorous damping matrix for finite element models with viscous behaviour. Computing, Bucarest, Rumanía 1993;5:1–4.
[7] Barbat AH, Oller S, Oñate E, Hanganu A. Viscous damage model for timoshenko beam structures. Int J Solids Struct 1997;34(30):3953–76.
[8] Barbat AH, Cervera M, Hanganu A, Cirauqui C, Oñate E. Failure pressure evaluation of the containment building of a large dry nuclear plant. Nucl Eng Des 1998;180(3):251–70.
[9] Cervera M, Hinton E. Non-linear analysis of reinforced plates and shells using a three dimensional model. In: Computational modelling of reinforced concrete structures. Swansea: Pineridge Press; 1986.
[10] Cervera M, Oliver J, Herrero E, Oñate E. A computational model for progressive cracking in large dams due to swelling of concrete. Eng Fract Mech 1990;35(1–3):575–85.
[11] Cervera M, Oliver J, Galindo, M. Simulación Numérica de Patologías en Presas de Hormigón. Monografía CIMNE no. 4, Barcelona, 1991.
[12] Cervera M, Oliver J, Galindo M. Numerical analysis of dams with extensive cracking resulting from concrete hydration: simulation of a real case. Dam Eng 1992;3(1).
[13] DiPasquale E, Çakmak AS. Detection and assessment of seismic structural damage. National Center for Earthquake Engineering Research, Technical Report NCEER-87-0015, State University of New York, Buffalo, 1987.
[14] DiPasquale E, Çakmak AS. On the relation between local and global damage indices, National Center for Earthquake Engineering Research, Technical Report NCEER-89-0034, State University of New York, Buffalo, 1989.
[15] DiPasquale E, Çakmak AS. Detection of seismic structural damage using parameter-based global indices. Probabilistic Eng Mech 1990;51(2):60–6.
[16] Faria R, Oliver J. A rate dependent plastic-damage constitutive model for large scale computation in concrete structures. Monograph CIMNE No. 17, Barcelona, 1993.
[17] Hanganu A, Oller S, Oñate E, Barbat AH. A finite element model for damage analysis of nuclear reactor containment shells. In: 2d National Conference on Boundary and Finite Element, Sibiu, Romania. 13–15 May, 1993.
[18] Hanganu A. Análisis no lineal estático y dinámico de estructuras de hormigón armado mediante modelos de daño, PhD Thesis, UPC, Barcelona, Spain, 1997.
[19] Hofstettter G, Mang AH. Computational mechanics of reinforced concrete structures. Editorial Vieweg; Vienna, Austria: 1995.
[20] Kachanov LM. Time of rupture process under creep conditions. Izvestia Akademii Nauk 1958;8:26–31 (in Russian).
[21] Kachanov LM. Continuum model of medium with cracks. J Eng Mech Div, ASCE 1980;106(EM5):1039–51.
[22] Kupfer HB, Gerstle KK. Behaviour of concrete under biaxial stresses. ASCE J Eng Mech Div 1973;99(EM4): 853–66.
[23] Lemaitre J. How to use damage mechanics. Nucl Eng Des 1984;(80):233–45.
[24] Lemaitre J. A continuous damage mechanics model for ductile fracture. J Eng Mater Tech 1985;107:83–9.
[25] Lybas J, Sozen M. Effect of beam strength and stiffness on dynamic behaviour of reinforced concrete coupled walls. Civil Engineering Studies, Structural Research Series No. 444, University of Urbana, Illinois, 1977.
[26] Lubliner J, Oliver J, Oller S, Oñate E. A plastic-damage model for concrete. Int J Solids Struct 1989;25(3):299–326.
[27] Lubliner L, Oller S, Oliver J, Oñate E. A plastic damage model for nonlinear analysis of concrete. Int J Solid Struct 1989;25(3):299–326.
[28] Lubliner J. Plasticity theory. New York: Macmillan Publishing Company; 1990.
[29] Mang H, Bićanić N, de Borst R. (Eds.) Computer modeling of concrete structures, Proc EURO-C, Innsbruck, Austria, 1994.

[30] Oliver J, Cervera M, Oller S, Lubliner J. Isotropic damage models and smeared crack analysis of concrete. Proc 2nd ICCAADCS, Zell Am See, vol. 2. Pineridge Press, Austria, 1990. p. 945–58.
[31] Oller S. Modelización numérica de materiales friccionales. Barcelona, Spain: Monograph CIMNE; 1991.
[32] Oñate E, Oliver J, Bugeda G. Finite element analysis of nonlinear response of concrete dams subject to internal loads. In: Bergan PG, Bathe KJ, Wunderlich W, editors. Europe-US Symposium on Finite Element Methods for Nonlinear Problems. Springer-Verlag; 1986.
[33] Oñate E, Oller S, Oliver J, Lubliner J. A constitutive model for cracking of concrete based on the incremental theory of plasticity. Eng Comput 1988;5:309–20.
[34] Oñate E. Cálculo de Estructuras por el Método de los Elementos Finitos, Centro Internacional de Métodos Numéricos en Ingeniería, CIMNE, Barcelona, 1992.
[35] Park Y-J, Ang AH-S, Wen YK. Seismic damage analysis and damage-limiting design of RC buildings, Civil Engineering Studies, Structural Research Series 516, University of Urbana, Illinois, 1984.
[36] Park Y-J, Ang AH-S. Mechanistic seismic damage model for reinforced concrete. ASCE, J Struct Eng 1985;111(4): 722–39.
[37] Simó JC, Ju JW. Strain and stress based continuum damage models—part I formulation. Int J Solids Struct 1987;23(7):281–301.
[38] Scotta R, Vitaliani R, Saetta A, Oñate E, Hanganu A. A scalar damage model with a shear retention factor for the analysis of reinforced concrete structures: theory and validation. Comput Struct 2001;79:735–55.
[39] Simó JC, Hughes T. Elasto plasticity, computational aspects. Berlin: Springer Verlag; 1995.
[40] Wastiels J. Behaviour of concrete under multi-axial stresses a review. Cem Concr Res 1979;9:35–44.
[41] Feenstra PH, de Borst R. A plasticity model and algorithm for mode-I cracking in concrete. Int J Numer Meth Eng 1995;38:2509–29.